Technical University of Denmark

Mapping localised freshwater anomalies in the brackish paleo-lake sediments of the Machile–Zambezi Basin with transient electromagnetic sounding, geoelectrical imaging and induced polarisation

Chongo, Mkhuzo; Christiansen, Anders Vest; Fiandaca, Gianluca; Nyambe, Imasiku A.; Larsen, Flemming; Bauer-Gottwein, Peter

Published in:
Journal of Applied Geophysics

Link to article, DOI:
10.1016/j.jappgeo.2015.10.002

Publication date:
2015

Document Version
Peer reviewed version

Mapping localized freshwater anomalies in the brackish Paleo-Lake sediments of the Machile-Zambezi Basin with transient electromagnetic sounding, geoelectrical imaging and induced polarization

Mkhuzo Chongo[1,*], Anders Vest Christiansen[2], Gianluca Fiandaca[2], Imasiku A Nyambe[3], Flemming Larsen[4] and Peter Bauer-Gottwein[1]

[1]Technical University of Denmark, Department of Environmental Engineering, Miljøvej, Building 113, 2800 Kgs. Lyngby, Denmark

[2]Aarhus University, Department of Geoscience, C.F. Møllers Alle 4, 8000-Århus C, Denmark

[3]University of Zambia, School of Mines, Department of Geology, Great East Road Campus, P.O Box 32379, Lusaka, Zambia

[4] Geological Survey of Denmark and Greenland (GEUS), Geochemistry, Øster Volgade 10, 1350 København K, Denmark

*Corresponding author email: mkhuc@env.dtu.dk

ABSTRACT

A recent airborne TEM survey in the Machile-Zambezi Basin of south western Zambia revealed high electrical resistivity anomalies (around 100 Ωm) in a low electrical resistivity (below 13 Ωm) background. The near surface (0-40 m depth range) electrical resistivity distribution of these anomalies appeared to be coincident with superficial features related to surface water such as alluvial fans and flood plains. This paper describes the application of transient electromagnetic soundings (TEM) and continuous vertical electrical sounding (CVES) using geo-electrics and time domain induced polarization to evaluate a freshwater lens across a flood plain on the northern bank of the Zambezi River at Kasaya in south western Zambia. Coincident TEM and CVES measurements were conducted across the Simalaha Plain from the edge of the Zambezi River up to 6.6 km inland. The resulting TEM, direct current and induced polarization data sets were inverted using a new mutually and laterally constrained joint inversion scheme. The resulting inverse model sections depict a freshwater lens sitting on top of a regional saline aquifer. The fresh water lens is about 60 m thick at the boundary with the Zambezi River and gradually thins out and deteriorates in water quality further inland. It is postulated that the freshwater lens originated as a result of interaction between the Zambezi River and the salty aquifer in a setting in which evapotranspiration is the net climatic stress. Similar high electrical resistivity bodies were also associated with other surface water features located in the airborne surveyed area.

Key words:

TEM; DCIP; Joint Inversion; surface water/ groundwater interaction; Zambezi River; Zambia

1 Introduction

The interaction between surface water and groundwater has been studied extensively around the world (Milosevic et al., 2012; Shanafield and Cook, 2014; Sophocleous, 2002; Westbrook et al., 2005; Winter, 1999; Zarroca et al., 2015; Zhou et al., 2014) using different approaches, and increasingly geophysical methods are being incorporated into such studies.

Specific examples of studies that have used geophysical data to investigate hydrogeological phenomenon include Bauer et al. (2006) who described the process of salt accumulation on islands within the Okavango Delta, related to the interaction between surface water and groundwater under evapo-concentration using a combination of electrical resistivity tomography (ERT) (which is the same as CVES with respect to geo-electrics) and hydrodynamic modeling; Sonkamble et al. (2014) who evaluated the extent of aquifer pollution from industrial effluent across the flood plain of the Palar River at Ambur Town (India) using 1D and 2D geo-electrics correlated with in-situ water quality data and ground penetrating radar; Shalem et al. (2014) who studied the interaction of the Alexander River with groundwater as it cuts its way across a mostly sandy Quaternary coastal aquifer on the eastern coast of the Mediterranean Sea; and Zarroca et al. (2014) who evaluated coastal discharge processes at the Peníscola marsh on the Spanish Mediterranean coast using electrical resistivity imaging and temperature, salinity and ^{224}Ra, ^{222}Rn tracer tests coupled with petrophysical analysis.

Thus geophysical techniques such as ERT are well suited for gathering data at high spatial resolution in comparison to for example point measurenments of hydrogeological parameters at sparsely spaced boreholes (Zarroca et al., 2014). An overall assessment strategy using a combination of different geophysical methods and traditional hydrogeological methods can therefore be advantageous (Brodie et al., 2007; Rubin and Hubbard, 2006). In this regard, TEM (Danielsen et al., 2003; Harthill, 1976; Nabighian, 1991; Xue et al., 2012), direct current geo-electrics (DC) (Aizebeokhai, 2010; Dahlin, 2001; Loke, 1999; Loke et al., 2013) and induced polarization (IP) (Bertin and Loeb, 1969; Dahlin et al., 2002; Fiandaca et al., 2012; Fiandaca et al., 2013; Titov et al., 2002) techniques are quite suitable for environmental and hydro-geological investigations particularly in sedimentary terrain.

Traditionally, TEM, DC and IP techniques have been deployed separately even for investigations at the same study site (Bauer et al., 2006; Ezersky et al., 2011; Guerin et al., 2001; Nassir et al., 2000; Vaudelet et al., 2011) although it is now common to have instrumentation that measures both DC and IP in the same field setup (Aristodemou and Thomas-Betts, 2000; Marescot et al., 2008). As a result, different types of datasets are quite often generated for the same physical or environmental phenomenon by inverting each type of dataset individually. Nevertheless, major benefits can be derived from joint inversion of different types of data that observe the same phenomenon and can lead to more accurate interpretations. Thus many studies have successfully used one form of joint inversion or another such as DC-TEM (Albouy et al., 2001; Christiansen et al., 2007; Danielsen et al., 2007), and MRS-TEM (Behroozmand et al., 2012; Vilhelmsen et al., 2014). Examples of DCIP joint inversions are scarce in the literature with the normal practice being to independently invert the DC and IP data either as separate inversion jobs or in one inversion job but without any of the datasets influencing the other during the inversion process. Furthermore, joint DCIP-TEM inversions have not been reported in the literature before. This paper therefore presents a first case study of joint inversion of DCIP-TEM data.

The focus of this paper is on local scale electrical resistivity anomalies derived from interpreting regional scale airborne TEM data in terms of surface water/groundwater interaction in the Machile-Zambezi Basin. The objectives were to describe the occurrence of high electrical resistivity anomalies in the low electrical resistivity background environment of the Machile-Zambezi Basin;

conduct local scale TEM and direct current-induced polarization (DCIP) CVES measurements along a transect cutting across an area exhibiting electrical resistivity anomalies; evaluate the benefits of joint inversion of the local scale TEM and DCIP data in comparison to separate inversions; and to evaluate the inverse resistivity section in terms of surface water groundwater interaction taking place at the local site.

2 Materials and methods

2.1 Study site

The study area is in the southern central low lying areas of the Machile-Zambezi Basin on the northern banks of the Zambezi River. The area is drained by three main tributaries of the Zambezi River namely Loanja, Machile (or Kasaya) and Ngwezi. The downstream reaches of the Machile and Ngwezi streams respectively flow across seasonally flooded plains as single channels before entering the Zambezi. However the Loanja stream terminates inland to form an inland delta or alluvial fan. The Loanja alluvial fan and the Simalaha flood plain (bound by Kasaya River to the west and the Zambezi River to the south) were the two local areas of interest for this study. However, the combined TEM/CVES transect is reported only for the Simalaha flood plain (Figure 1).

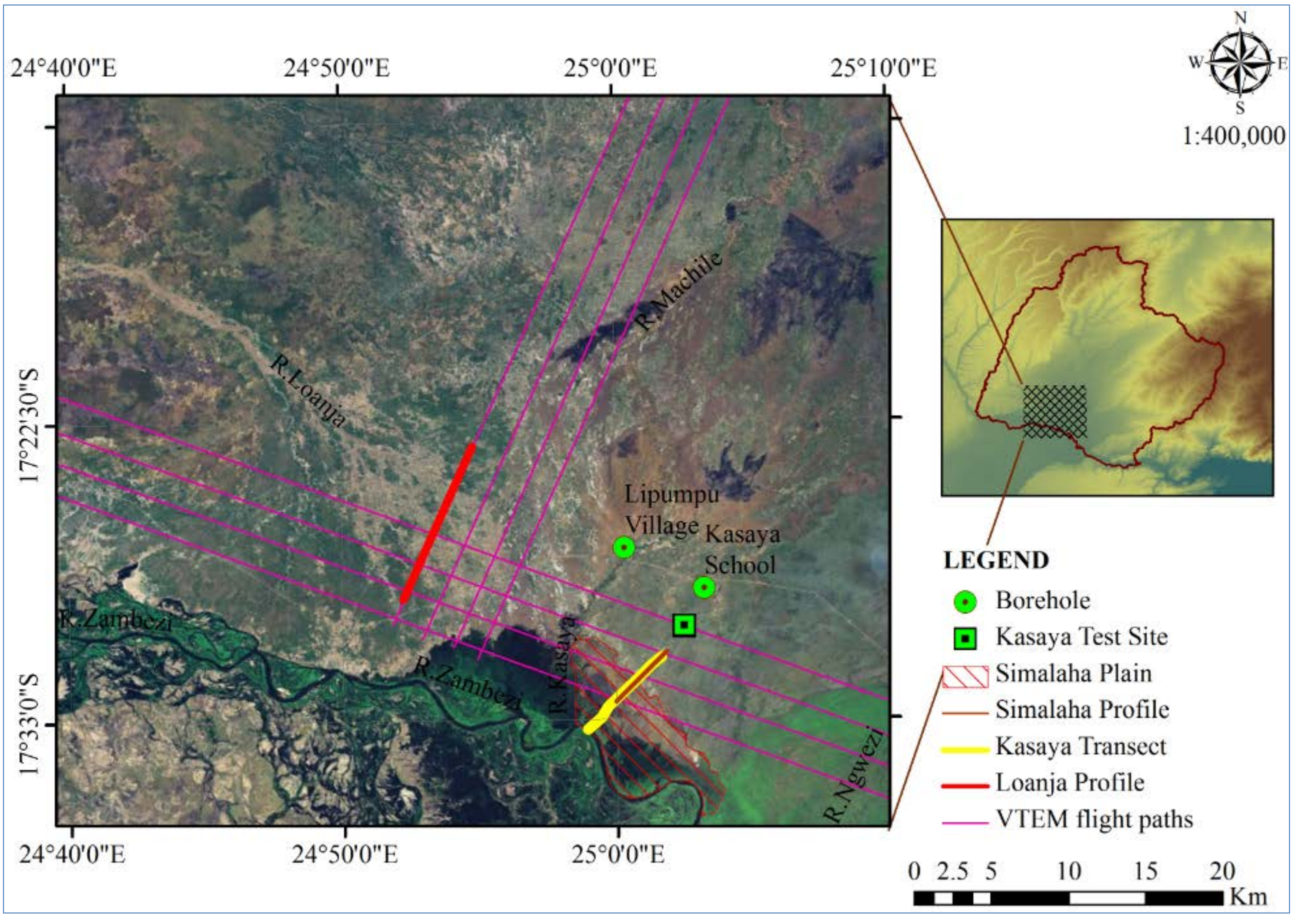

Figure 1: The study area depicting Loanja alluvial fan, Simalaha flood plain, Kasaya Transect and TEM flight paths. Satellite image courtesy of ESRI (2014). Note that the Simalaha Profile is shorter than the Kasaya Transect since there is no more airborne electromagnetic data outside the flight lines, whereas the CVES and TEM data on the Kasaya Transect extend beyond the flight path where the Simalaha Profile ends up to the Zambezi River.

2.2 Data collection and pre-processing

Airborne data was conducted along 8 flight lines totalling 1000 line kilometres using the VTEM system (GEOTECH, 2011). Four of the flight lines were oriented southwest to northeast whereas the other 4 were oriented from northwest to southeast (Figure 1 in Section 2.1). Details about the airborne survey and about the processing, inversion and interpretation of the collected TEM data are given in Chongo et al. (2015). Cross sections of the airborne TEM data along the Loanja and Simalaha profiles (Figure 1 in Section 2.1) are shown in Figure 2 (a.) and (b.) respectively. These depict superficial electrical resistivity anomalies in an otherwise low electrical resistivity background (saline environment) and were the basis of the detailed local scale study conducted on the Kasaya transect presented in this paper.

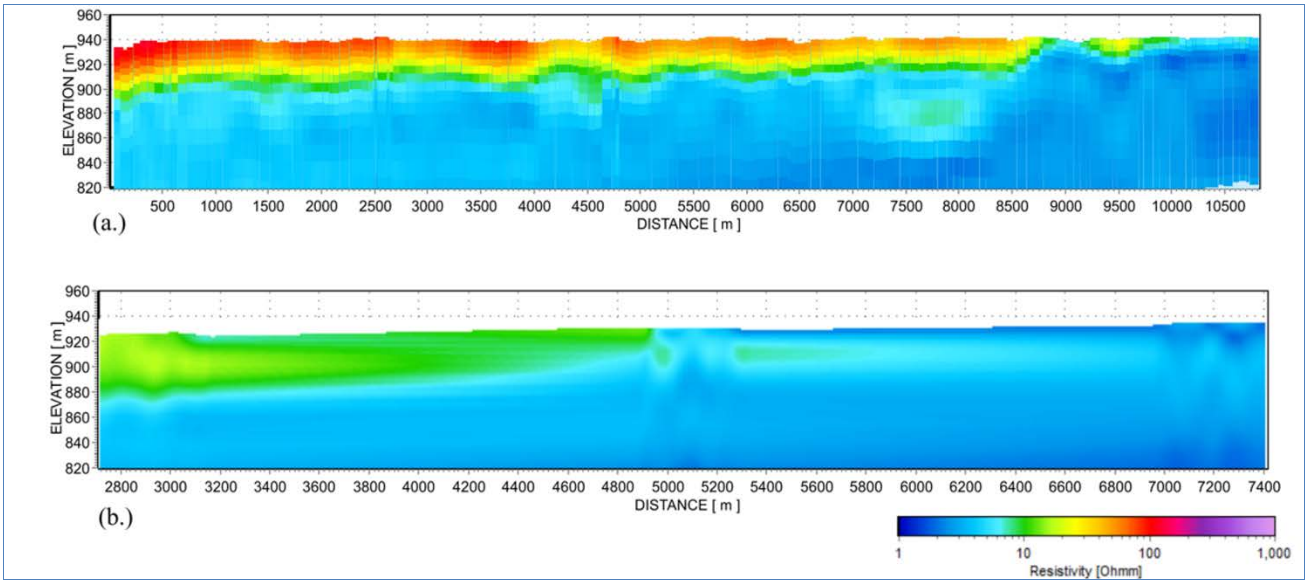

Figure 2: (a) Electrical resistivity cross section along Loanja Profile (Figure 1 in Section 2.1) from the airborne transient electromagnetic data. (b) Interpolated electrical resistivity cross section along Simalaha Profile (Figure 1 in Section 2.1) from the airborne TEM data. Note that Loanja and Simalaha profiles are not drawn to scale nor are they the same length since Loanja Profile (about 106 km long) is along a flight line whereas Simalaha Profile (about 5.7 km long) cuts across flight lines and as a result has a more limited data extent.

The detailed local scale geophysical investigation conducted across the Simalaha Plain at Kasaya (Figure 1 in Section 2.1) comprised:

i. 6.6 km of CVES (Loke, 1999; Loke et al., 2013; Nassir et al., 2000) measurements at 5 m electrode spacing using the gradient array (Dahlin and Zhou, 2006) with 25,003 data points. The Terrameter LS (ABEM(a), 2012) was used for the CVES to measure both direct current electrical resistivity (DC) (Loke et al., 2013) and time domain induced polarisation (IP) (Johnson, 1984) hence the term DCIP to denote the combination of DC and IP measurements in a roll-along setup (information on the transmitter and receiver characteristics of the Terrameter LS is given in Section 2.3 below); and
ii. 64 single site TEM (Christiansen et al., 2006) soundings using the Aarhus University/ABEM WalkTEM system; and another set of 64 central loop TEM soundings using the Geonics ProTEM 47D instrument (Geonics, 2006) at the same positions as the WalkTEM soundings. Thus the total number of TEM soundings along the transect line was 128 spaced at approximately 100 m along the 6.6 km transect line per pair of WalkTEM/ ProTEM 47D soundings (information on the transmitter and receiver characteristics of the WalkTEM is given in Section 2.3 below). However data from the ProTEM instrument was not used for this paper.

The DCIP data was pre-processed by removing all data points with negative electrical resistivity and data variations greater than 1.5 %. The data that was removed this way represented only 3.3 % of the original data –i.e. 851 filtered out measurements from a total of 25, 857 DCIP measurements. The data set was then imported into the Aarhus Workbench with the IP data gated into 10 channels. Data processing in the Workbench comprised semi-automatic removal of bad IP data by setting a maximum slope change for the IP decay curves followed by visual inspection of the DC and IP data points along the profile and consequent disabling of the outliers. The DCIP noise model was set to 1.03 uniform standard deviation (USTD) on DC and 1.15 USTD on IP whereas the threshold on voltage was set to 2.0 mV. For the WalkTEM data we used data from 77.6 µs to 2.84 ms, focusing on the deep information only.

2.3 Instrumentation

As mentioned above, the geophysical equipment used for this paper comprised the Terrameter LS for geo-electric measurenments and the WalkTEM for transient electromagnetic measurenments. Waveform characteristics for the Terrameter LS (ABEM(a), 2012) and the WalkTEM (ABEM(b), 2014) are outlined below in sections 2.3.1 and 2.3.2 respectively.

2.3.1 Terrameter LS waveform characteristics

The transmitter waveform of the Terrameter LS was in the form of a square wave and comprised a positive and a negative pulse as shown in Figure 3. The period of the transmitter waveform was automatically determined by the Terrameter LS to be 6.15 s taking into account the power line frequency of 50 Hz and DC delay and acquisition times of 0.4 s and 0.6 s respectively and the time needed to perform the chargeability measurenments. Thus the transmitter waveform was characterized by a 1 s positive pulse, followed by an off time of 1.77 s and then a negative pulse also of 1 s duration followed by an off time of 2.38 s. IP measurenments were performed during both off times. Self-potential measurenments on the other hand were conducted only during the second off time hence its longer duration. Each measurement comprised at least two cycles so that measured voltages could be averaged in order to eliminate zero shift and linear drift during the measurement cycle (ABEM(a), 2012). Furthermore, the shape of the transmitter waveform prevented polarization from occurring at the electrodes in addition to removing any background voltage or self-potential (Binley and Kemna, 2006).

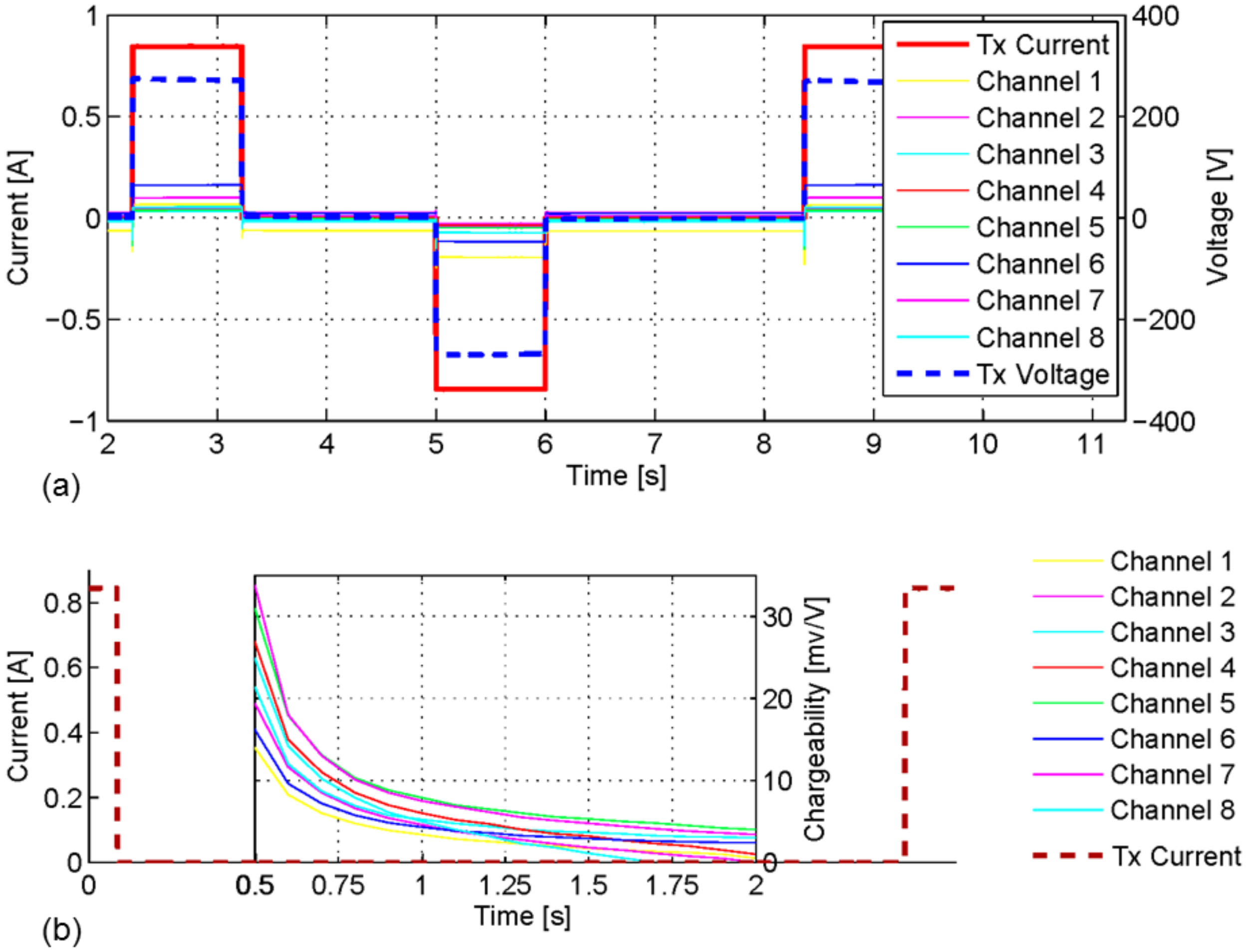

Figure 3 (a) Terrameter LS transmitter current and voltage waveforms and input voltages from various input channels based on the 4 electrode configuration. (b) Induced polarization decay curves from the various channels of the Terrameter LS measured during transmitter current off time.

The Terrameter LS is a multichannel auto switching instrument which when compared to instruments with separate transmitter/ receiver units has low power, voltage and current ratings of not more than 250 W, 1 000 V and 3 Amperes respectively. This is in contrast to the 3 000 V/ 10 A reachable with separate transmitter/ receiver instruments. However, multichannel auto switching instruments allow for more freedom in the array selection for using arrays with small geometrical factor values (e.g. the gradient array) in comparison with instruments with separate transmitter/ receiver units (i.e. the dipole-dipole configuration). The low geometrical factor values imply higher

IP voltages sampled by the instruments which partly compensates for the smaller injected current (Gazoty et al., 2013). In addition, processing of the full-decay IP data (as was the case for this paper) allows for the effective deletion of spurious decays such that in the end there is reliable data with multichannel auto-switching instruments also in addition to tomographic coverage.

2.3.2 WalkTEM waveform characteristics

The WalkTEM instrument utilises a short duration (about 10 ms) current pulse to induce eddy currents into the subsurface which in turn generate secondary electromagnetic fields that can be detected by a receiver coil placed at the surface (ABEM(b), 2014; Christiansen et al., 2006; Nabighian, 1991). Characteristic waveforms and earth responses for a TEM sounding depicting the low moment and high moment curves are shown in Figure 4. The low moment is designed obtaining information about the conductivity structure of the shallow subsurface whereas the high moment provides information about the conductivity structure of the deeper subsurface.

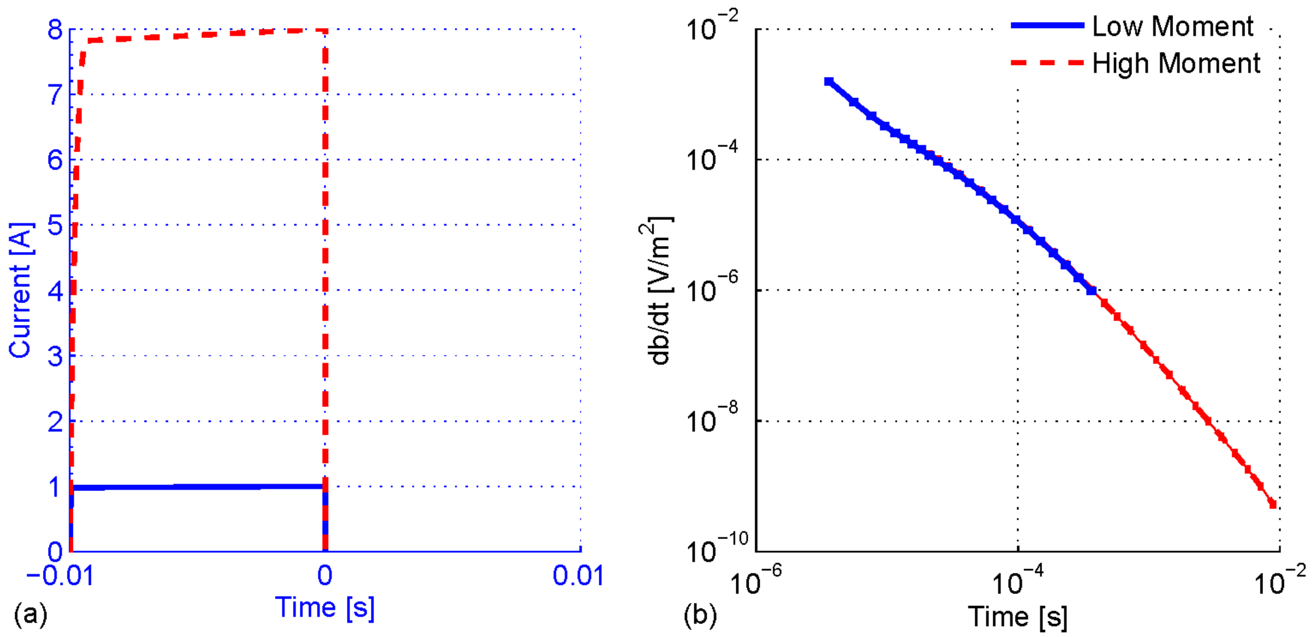

Figure 4: (a) WalkTEM transmitter waveform; and (b) Typical earth response.

2.4 Inversion methodology

DC and TEM data were inverted separately using the 1D laterally constrained inversion (LCI) (Auken et al., 2005) scheme. Subsequently, a joint inversion using the mutually and laterally constrained inversion scheme of Christiansen et al. (2007) was conducted on the DC and TEM data as a single inversion. This was then extended to include IP data using the Cole-Cole model setup (Fiandaca et al., 2012; Gazoty et al., 2012b) so that the final inversion was a joint inversion of DCIP and TEM data. Thus the DCIP and TEM model parameters being modelled comprised (intrinsic chargeability (M_0), frequency dependence constant (c), time constant (τ), formation electrical resistivity (ρ) and layer thicknesses). The inversion algorithm Aarhusinv (Auken et al., 2014) was used for all inversions presented in this paper.

As mentioned in Section 2.2, the interval of TEM soundings along the Kasaya transect was approximately every 100 m whereas the DCIP data was collected with 5 m gradient array electrode spacing. The lateral constraints on the TEM models were setup such that each TEM model was constrained only to the adjacent TEM model on either side along the transect line. Similarly, each DCIP model was constrained only to the adjacent DCIP models. Treatment of mutual TEM/DCIP constraints is explained below.

The reference lateral constraint on electrical resistivities was set to 0.3 and scaled according to:

$$C_i = C_r * \sqrt{\frac{d}{d_r}} \qquad (1)$$

where C_i = lateral constraint on resistivity [dimensionless fraction]; C_r is the reference constraint [dimensionless fraction]; d is the distance between respective models [m]; and d_r is the reference distance which was set to 10 m. Furthermore, the reference constraint on depths was set to 1 m and scaled according to depth so that the deeper layers had relatively tighter constraints. The constraint values mentioned above can be considered as medium for the resistivity values and tight for the depths. These were used because they were found to give a reasonable inversion result using trial and error procedure.

Lastly, mutual constraints were applied between the TEM and DCIP models using depths of layers to set the constraint width and scaled according to the power law given above (equation 1). Thus, the deeper layers had wider and tighter constraints between TEM and DCIP models because the constraints were only applied if the distance between respective TEM and DCIP models was less than or equal to the layer depth. The reference constraint between TEM and DCIP models was set to 0.1 but the reference depth was the same as for the lateral constraints (Christiansen et al., 2007).

2.5 Petro-physical considerations

The petro-physical relation for the Kasaya area was estimated using the following equations (Kirsch, 2009; Mualem and Friedman, 1991; Rhoades et al., 1989),

$$\sigma_o = \frac{\sigma_w * \theta^u}{\emptyset} + \sigma_{sfc} \quad (2)$$

$$\sigma_{sfc} = 1000 * (2.3 * C - 0.021) \quad (3)$$

Where σ_o = bulk conductivity or formation conductivity [µS/cm]; σ_w = pore water conductivity [µS/cm]; θ = volumetric water content [dimensionless]; u = exponent on volumetric water content (reported as 2.5 by Kirsch (2009)) ϕ = porosity [dimensionless]; σ_{sfc} = surface conductivity [µS/cm]; and C = volumetric clay content [dimensionless] (Kirsch, 2009). The constant 1000 is a unit conversion factor from mS/cm to µS/cm whereas the constants 2.3 and 0.021 are empirical factors as derived by Rhoades et al. (1989).

For fully saturated conditions applicable to groundwater, the volumetric water content was taken to be the same as the porosity meaning that Equation 2 could be simplified as:

$$\sigma_o = \sigma_w \emptyset^v + \sigma_{sfc} \tag{4}$$

where the porosity exponent, $v = u - 1$ (5)

The various parameters of equation 2 and 3 (porosity, porosity exponent and clay content) were adjusted in order to obtain the best curve fitting through the Kasaya pore water point and the unsaturated formation resistivity point Figure 3 (a.). The Kasaya pore water point was defined by the pore water conductivity measured from the borehole fluid by Banda et al. (2014) using an electrical conductivity meter, and the formation electrical resistivity below the water table as measured by the TEM method. The layered earth model derived from 1D inversion of the TEM sounding at Kasaya was comparable to the induction borehole log of Banda et al. (2014) at the Kasaya School borehole Figure 3 (b.). The TEM sounding was conducted using a 40 x 40 m central loop configuration with the centre of the loop coincident with the borehole. The unsaturated formation resistivity point was defined by a pore water electrical conductivity of 0 µS/cm, denoting absence of pore water, and the formation electrical resistivity above the water table as measured by the TEM method.

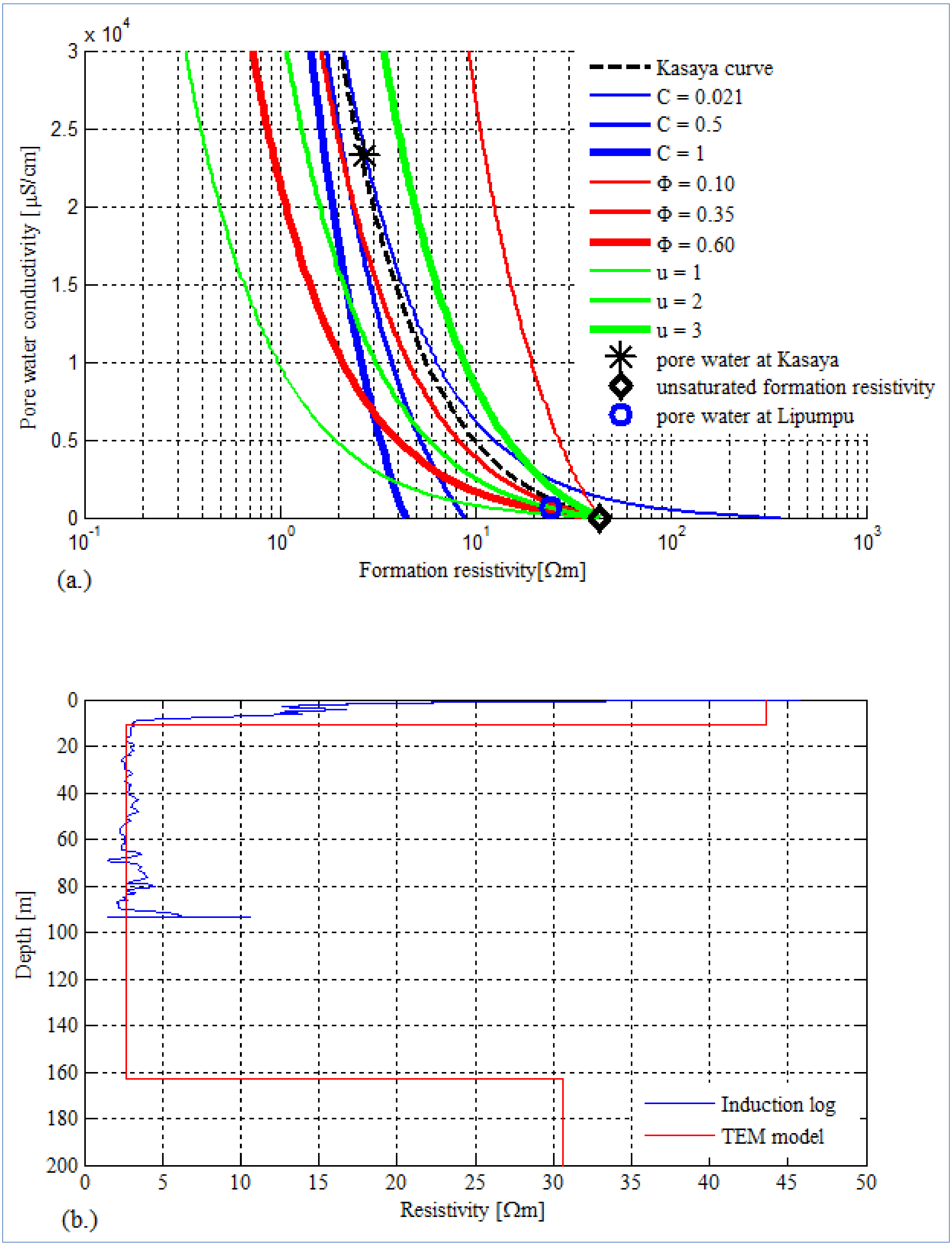

Figure 5: (a.) Illustration of the variation of the petro-physical relation (Equation 1) for different parameters (porosity (ϕ), volumetic water content exponent (u) and clay content (C). Kasaya curve

is the curve fitting the measured borehole fluid conductivity at Kasaya and the unsaturated formation resistivity measured by TEM at the same location. (b.) Variation of electrical resistivity with depth from an induction log and TEM sounding at Kasaya School in Machile-Zambezi Basin.

At present, a petro-physical relationship between IP parameters and hydrogeological parameters is difficult to define. However, Pelton et al. (1978) observed that chargeability (Cole-Cole parameter M_0) and time constant (Cole-Cole parameter τ) were directly proportional to fluid concentration and that grain size was inversely proportional and directly proportional to M_0 and τ respectively. On the other hand, Slater and Lesmes (2002) using an experimental laboratory freshwater intrusion into salty water model observed that the chargeability was directly proportional to the fluid resistivity –i.e. inversely proportional to the fluid conductivity in contrast to observations by Pelton et al. (1978). Furthermore, Slater and Lesmes (2002) could not find any clear correlation between chargeability and clay content for various mixtures of sand and bentonite clay. However, a correlation was found to exist between clay content and the product of fluid conductivity and chargeability.

Given the observations by Slater and Lesmes (2002), the petro-physical relation given by Equation (2) is assumed to hold for this study, given that the electrical resistivity models produced from the joint DCIP-TEM inversion are informed or constrained by the chargeability models. Further research is required for better treatment of IP parameters with respect to hydrogeological considerations (Gazoty et al., 2012a; Gazoty et al., 2012b; Weller et al., 2013).

2.6 Depth of investigation

The depth of investigation (DOI) (Christiansen and Auken, 2012; Oldenburg and Li, 1999; Roy and Apparao, 1971; Spies, 1989) can be used as a way of evaluating the degree to which measured data and their associated uncertainty or noise level are able to resolve the parameters of an inverse layered earth model (Christiansen and Auken, 2012). In this paper, DOI estimation was based on recalculation of the Jacobian matrix of the final 1D inverse model, taking into account the full system transfer function, system geometry, the data and the noise level on the data (Christiansen and Auken, 2012), but not taking into account in the computation the model regularization. From the Jacobian matrix, cumulated sensitivities were computed from which the DOI was deduced based on an empirical cumulative sensitivity threshold value or global threshold (Christiansen and Auken, 2012). Two global threshold values were used in this paper: 0.75, for deeper estimation of DOI (or lower DOI) and 1.5, for shallower estimation of DOI (or upper DOI). It should be noted that different DOIs will result for inverse models from different data types based on the same global threshold because the sensitivities of the different data types do not behave in exactly the same way. For example, DC data have higher sensitivities for the shallower subsurface whereas TEM data are more sensitive to conductive layers at greater depth (Christiansen and Auken, 2012). The DOI is presented on the model cross sections in form of colour fading with the upper DOI having a slightly darker shade than the lower. Thus model parameters above the DOI can be said to be well resolved whereas those below it are not. In addition to DOI, data residuals are also typically used as a measure of the fit between the data and the model although the information contained in the data residuals is also implied in the DOI.

3 Results and discussion

As mentioned in Section 2.2, the airborne survey results show electrical resistivity variations correlated with surface water features in both the Simalaha Plain and the Loanja Alluvial Fan (Figure 1 and Figure 2). However, only the results of the Simalaha Profile survey are tackled in this paper.

3.1 Separate inversions

LCI of DC (Figure 6 a.) data resulted in a detail of electrical resistivity variations and clearly delineated a conductive layer about 5 m thick on top of a high electrical resistivity lens that thins out from left to right –i.e. south to north– with respective lowering of electrical resistivity values. The DOI could not go beyond the high resistivity lens especially where the lens was thick and the resistivities relatively very high, but was able to penetrate comparatively deeper where the high resistivity lens had thinned out. In addition, the DOI was very variable along the model cross section and was typically very shallow at both ends, but mostly a few meters less or more than 40 m. The shallow DOI at both ends is a consequence of lack of data in the deeper parts as a result of the four electrode configuration which has a shallower penetration depth for shorter electrode spacing.

LCI of TEM (Figure 6 c.) data shows reduced detail of electrical resistivity variations but improved resolution of electrical resistivity interfaces at depth. The TEM is able to look beyond the high resistivity lens with a much deeper DOI, meaning that model parameters are resolved at larger depths with the TEM data. In addition, the DOI varies more uniformly being deeper at the beginning of the transect line (around 100 m) and shallower at the end (around 50 m). This variation of DOI is indicative of the sensitivity of the TEM method to conductive layers at depth. At the beginning of the transect line, the resistive lens is thicker and therefore the depth to the conductive layer is deeper than at the other end of the transect line, where the resistive lens is thinner and the depth to the conductive layer is shallower.

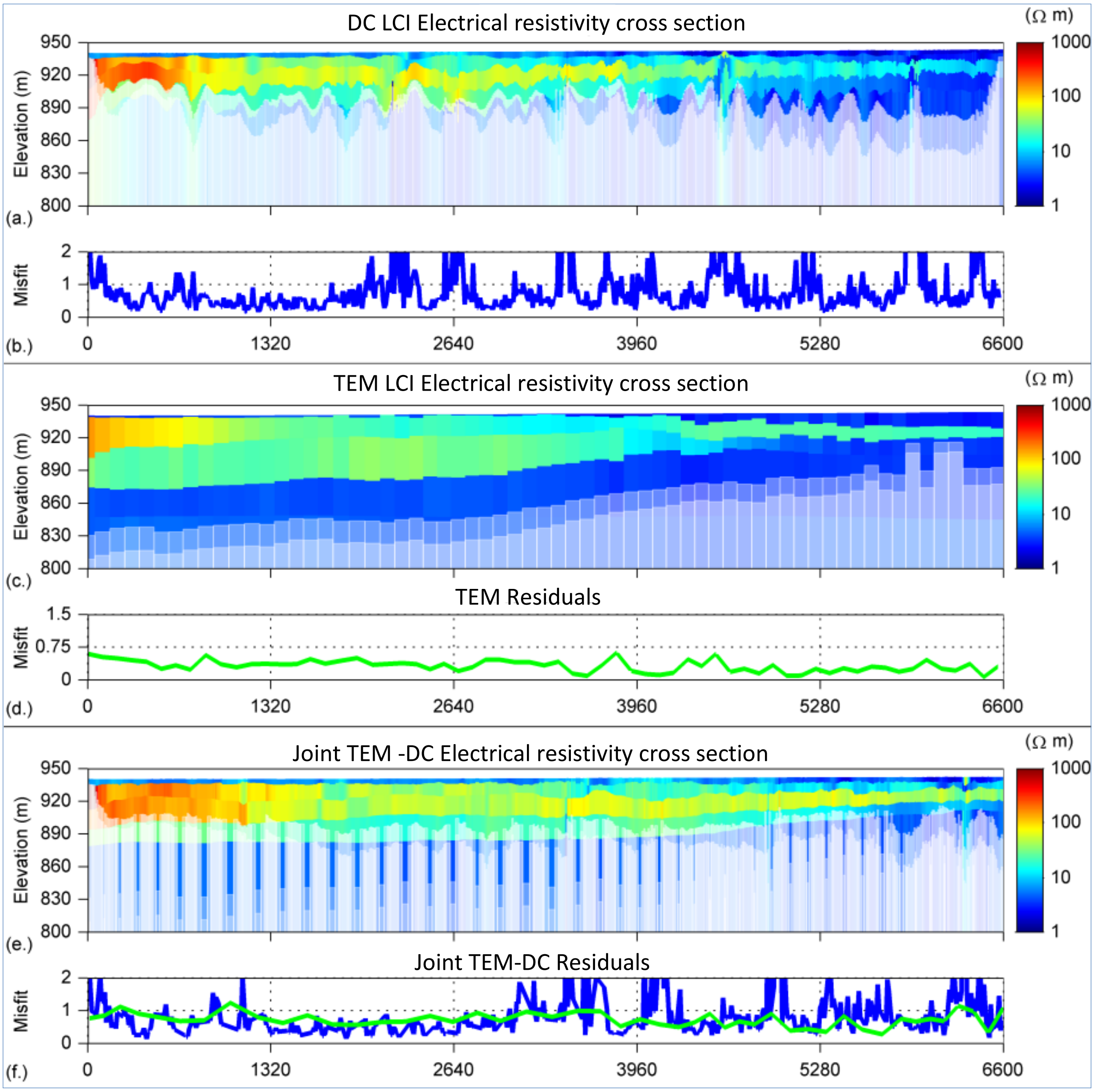

Figure 6: Inverse electrical resistivity cross sections and residual plots. (a.) – (b.), inverse electrical resistivity cross section and residual plot respectively for LCI of DC data; (c.) – (d.), inverse electrical resistivity cross section and residual plot respectively for LCI of TEM data; and (e.) – (f.),

inverse electrical resistivity cross section and residual plot respectively for MCI-LCI (i.e. joint inversion) of DC and TEM data. On the residual plots, blue lines are for DC residuals whereas green lines are for TEM residuals.

3.2 Joint TEM-DC inversions

Evaluation of the inversion result from joint inversion of DC and TEM data (Figure 6 (e.) in Section 3.1) shows that major benefits can be derived when TEM and DC data are incorporated into the same inversion job. Variation of DOI for the DC models became much more uniform although it remained at more or less the same level as with the DC only LCI. However, the determination of the depths of different electrical resistivity layers showed a marked improvement in the DC models, which indicates that the characteristic of TEM data to clearly determine layer depths migrated into the DC models during the inversion process. Furthermore the TEM inverse models from the joint inversion still showed a deeper DOI in addition to being in good agreement with the DC data in the upper parts of the section (Figure 6 (e.) in Section 3.1). Thus CVES data was able to improve the resolution of TEM data in the shallow subsurface, whereas TEM data was able to improve the determination of depths, resistivities and thicknesses in the DC data throughout the transect line.

3.3 Joint TEM DCIP inversions

The results of the Joint TEM-DCIP inversion are shown in Figure7 and Figure 8, with respect to electrical resistivity and chargeability distributions along the Kasaya transect line. Other additional parameters (τ and c), with the potential of further characterising the aquifer and sediments at Kasaya, were also produced from the DCIP-TEM joint inversion. However these have not been presented or tackled in this paper as doing so would require substantial additional research and analysis beyond the scope of the current study.

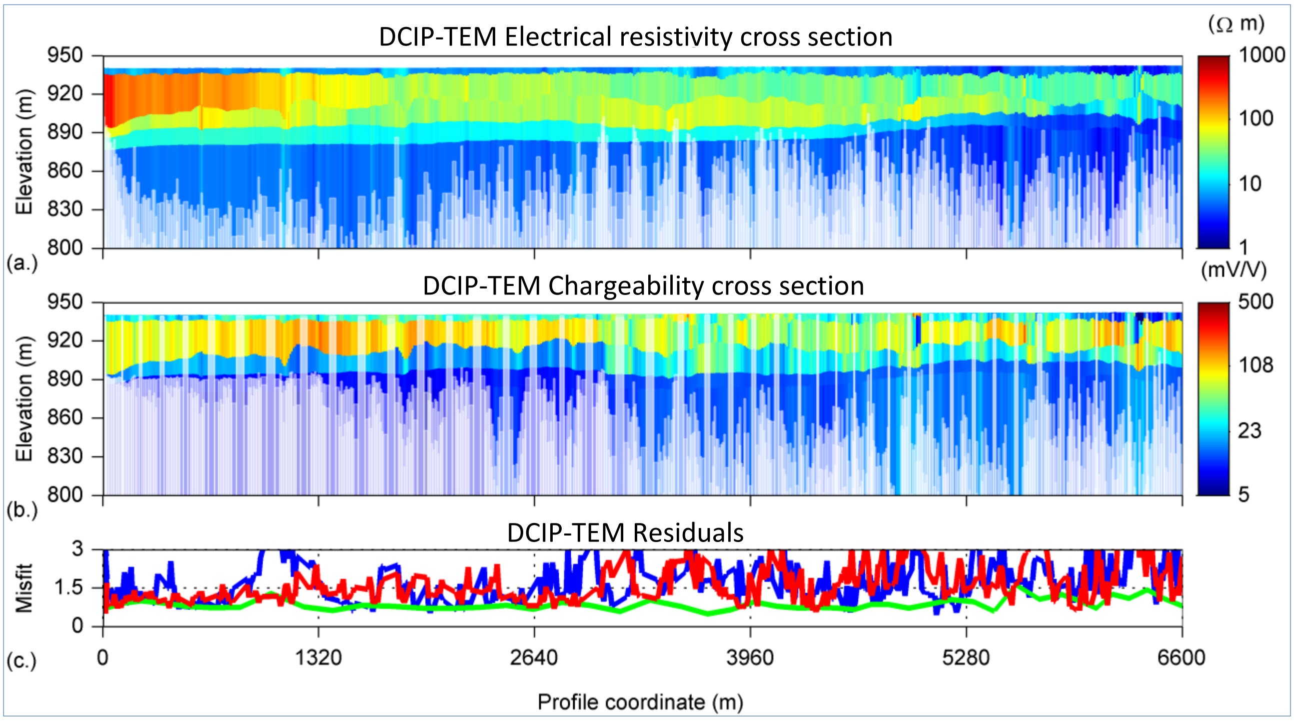

Figure 7: (a.) Inverse electrical resistivity cross section, (b.) inverse chargeability cross section, and (c.) data residual plot from joint inversion of DCIP and TEM data. The green line is for TEM residuals whereas the blue and redlines are for DC and IP residuals respectively.

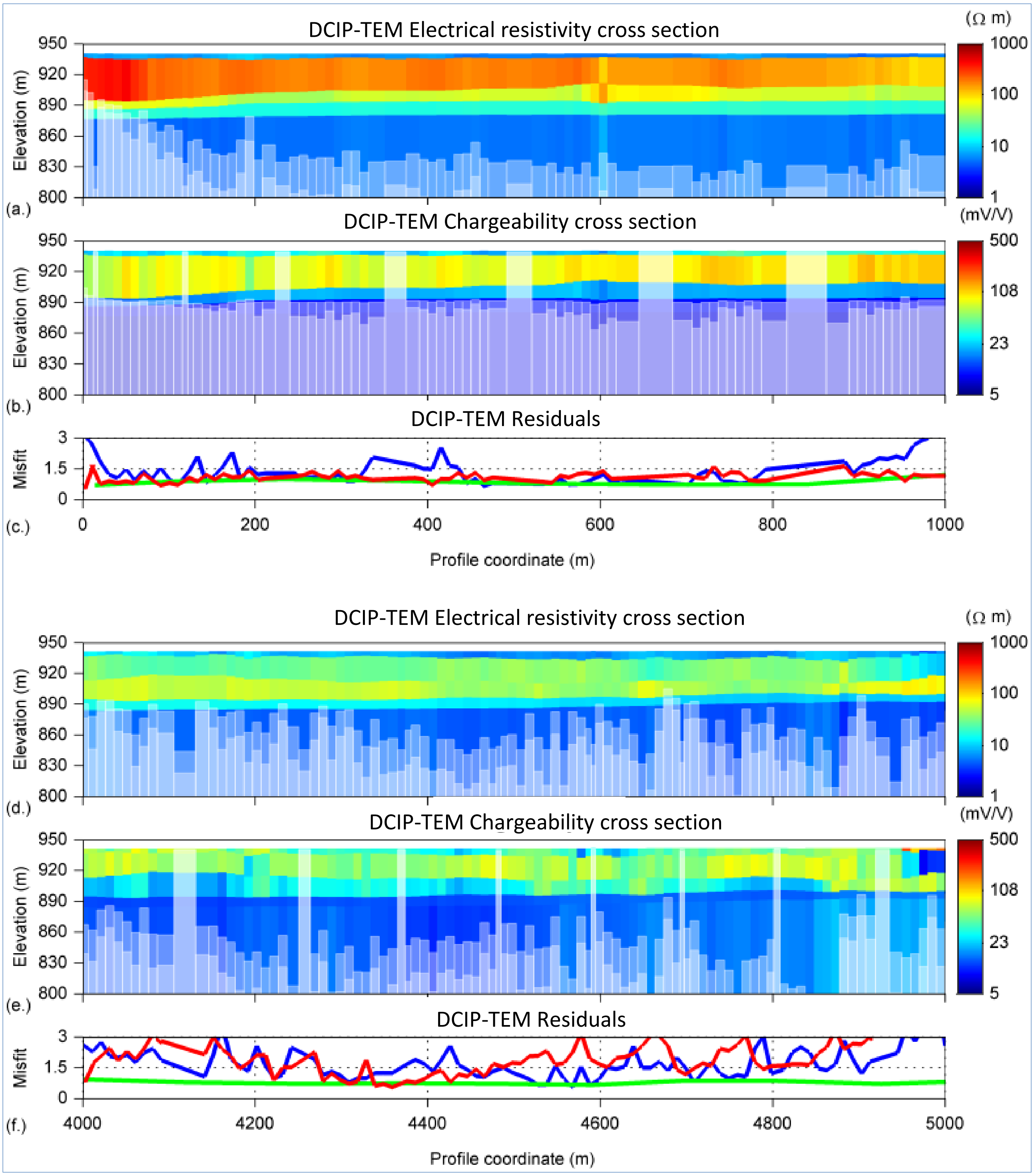

Figure 8: (a.) – (c.) zoom in inverse electrical resistivity cross section, inverse chargeability cross section, and data residual plot respectively from joint inversion of DCIP and TEM data for distance interval 0 – 1,000 m. (e.) – (f.) zoom in inverse electrical resistivity cross section, inverse

chargeability cross section, and data residual plot respectively from joint inversion of DCIP and TEM data for distance interval 4,000 – 5,000 m.

Thus the model cross sections from joint DCIP-TEM inversion (Figure 7 and Figure 8) show:

i. a low electrical resistivity layer about 5 m thick with electrical resistivity values ranging between 1 - 12.6 Ωm at the top;
ii. a middle high electrical resistivity lens which is about 60 m in the south (left hand side) and thins out towards the north (right hand side) to about 22 m where an electrical resistivity gradient of 200 to 30 Ωm is observed from south to north respectively.
iii. the high electrical resistivity lens underlain by a transition layer with thickness ranging between about 5 to 10 m and electrical resistivity values in the range of about 15 Ωm. This layer diminishes at about 4600 m from the beginning of the transect line.
iv. formation resistivity of around 3.6 Ωm below the high electrical resistivity and transition layers.
v. an inverse chargeability model with three distinct layers in the first half of the section and a heterogeneous mix of chargeability in the second half. Between 0 to about 3,300 m an approximately 5 m thick 20–40 mV/V chargeability layer overlies a 90 – 120 mV/V chargeability layer with variable thickness of about 20-40 m. This in turn is underlain by a 15-20 mV/V chargeability layer below which the chargeability values are about 7 mV/V. After 3,300 m the chargeability section is more or less mixed or chequered and shows a lesser degree of layering. Chargeability values below the chequered section are about 10 mV/V.

The distribution of chargeability along the Kasaya Transect appears to be an indication of the layering of the sediments along the transect line in addition to being correlated with the electrical resistivity distribution in a manner similar to the experiment of Slater and Lesmes (2002). The chargeability therefore had an added value of defining the stratification and zones where freshwater possibly infiltrated and replaced salty groundwater. Furthermore it should be understood that the main benefit of integrating DC, TEM and IP data all together is to obtain a unique model where the geometry and parameter values are defined by all the available information. Thus the resulting models are data driven in both the shallow part (due to DCIP data) and at depth (as a result of the TEM data). Thus this is not a matter of DOI only and an attempt to give an augmented interpretation in terms of changes in electrical resistivity and IP due to changes in fluid conductivity with reference to the petro-physical/ textural considerations of the study area is given below.

In the experiment of Slater and Lesmes (2002), a sample of de-aired sand was first saturated with pure water (electrical resistivity = 1000 Ωm) and then flushed with 33 pore volumes (25 l x porosity) of NaCl (electrical resistivity = 4.54 Ωm) followed by gradual reintroduction of 37 pore volumes (27 l x porosity) of pure water. Measurements of electrical resistivity and chargeability were performed during the initial introduction of NaCl solution and the reintroduction of pure water. From this, Slater and Lesmes (2002) observed that the bulk or formation electrical resistivity reduced with the introduction of saline water and recovered with the reintroduction of pure water. They also noticed that the chargeability increased with fluid electrical resistivity in such a way that the chargeability curve was almost a mirror of the electrical resistivity curve. Thus, the fact that the high chargeability distribution along the Kasaya transect appears to coincide more or less with the high electrical resistivity distribution suggests that processes similar to those modelled by Slater and Lesmes (2002) are at play in the Kasaya area. In other words, the high chargeability observed along the Kasaya transect has to more to do with the infiltration of fresh water into a pre-existing saline environment. The high chargeability section would therefore be an indicator of the physical extent of where salty water has been replaced by recent fresh water. This concept of fresh water replacing pre-existing saline groundwater water under through flow conditions is also supported by Banda et al. (2015) through their sediment dilution experiment in which 20 g of drill core sediment samples from the Machile-Zambezi Basin were placed in 50 ml centrifuge tubes and filled with deionised water. They then placed the tubes in a mechanical shaker in order to dissolve mineral phases until equilibrium was reached after which deionised water kept being replaced in the centrifuge tubes until the electrical conductivity was almost zero, indicative of complete removal soluble salts. Nevertheless this interpretation would benefit from borehole verification through measurenments of EC values and other hydrogeological data along the Kasaya Transect. However site conditions at the time of the geophysical survey prevented the deployment of machinery or equipment needed for the drilling of boreholes. Lack of access roads coupled with swampy conditions during the rainy season meant that any form of drilling was nearly impossible.

3.4 Hydrogeological interpretation

Available borehole records for the Kasaya area (Kameyama (2003) and Banda et al. (2014)) indicate that the main aquifer material is composed of mixed and alternating sequences of sand and clay. Nevertheless comparison of a coincident TEM sounding with the borehole record and induction log at Kasaya (Figure 5 b) indicates that the alternating sequences of sand and clay below the water table are seen as one layer with average resistivity of 3 Ωm. Above the water table the formation resistivity of the unsaturated zone was determined as 44 Ωm (resistivity standard deviation factor = 1.07, i.e. ± 3 Ωm) from the TEM inverse layered earth model. The interface between the 44 Ωm layer and the 3 Ωm layer at 10.6 m (depth standard deviation factor = 1.01) was taken to represent the water table although the water level reading in the borehole record at Kasaya indicates the water table to be at 13.2 m. The difference in depth between the water table recorded in the Kasaya borehole record and the one inferred from the TEM sounding could be as the result of either systematic and random errors when the water table was measured or the effects of the capillary fringe or a combination of both factors; it might also just be that the TEM method is not very accurate at making quantitative estimates of the water table. Nevertheless the induction log profile appears to be in agreement with the TEM sounding (Figure 5b) and given the low standard deviation factors on both the electrical resistivity and the depth, the 1D electrical resistivity model derived from the TEM sounding is considered to be very precise.

Rhoades et al. (1992) classified non saline water as having electrical conductivity (EC) of less than 700 µS/cm, with anything above this threshold falling into one of five other degrees of salinity with the highest being the category of brines having EC greater than 45000 µS/cm. Therefore based on equation 2, freshwater aquifers in the Kasaya area can be considered to have a formation resistivity of greater than or equal to 29.4 Ωm; 5.6 – 29.4 Ωm for slightly to moderately saline groundwater; and 5.6 Ωm or less for very saline groundwater (Zarroca et al., 2011). This classification of aquifer salinity should be viewed as representing the order of magnitude, since the petro-physical relation is bound to be site specific depending on the distribution of clay content and porosity. It can be seen from the measured pore water conductivity at Lipumpu Village, which falls at its own unique position different from the petro-physical considerations at Kasaya (Figure 5a). Therefore, the top 5 m layer with heterogeneous resistivity values ranging between 1 - 12.6 Ωm is probably a layer of moist top soil with varying degrees of porosity, clay content and water content; the localised lower electrical resistivity values being attributed to higher localised clay content compared to areas with higher localised electrical resistivity. In addition, the high electrical resistivity lens, below the 5 m top soil layer, shows resistivity values greater than the 44 Ωm threshold for non-conducting pore water, within 1800 m from the edge of the Zambezi River. A possible explanation is that this region is composed of coarser textured sediments (sand) whose bulk electrical resistivity is governed primarily by the pore water conductivity in comparison with clayey materials whose bulk electrical resistivity is also influenced by the salts retained on the surface of the clayey minerals (Zarroca et al., 2011). Therefore the surface conductivity component of equation 1 would be significantly reduced leading to a rise in formation conductivity above the 44 Ωm for non-conducting pore waters. Beyond 1800 m from the edge of the Zambezi River, the petro-physical relation appears to hold with electrical resistivity values around 30 Ωm indicative of freshwater. Below the fresh water lens, the petro-physical relation suggested by equation 1 also holds and with electrical resistivity values all below 3 Ωm; this part of the aquifer is expected to have pore water conductivity above 20,000 µS/cm. This distribution of electrical resistivity values along the Kasaya transect, into three distinct zones, indicates infiltration of fresh surface water into a pre-existing saline aquifer. The interaction of surface water and ground water as suggested by the geophysics is conceptualised in Figure 7, and is probably driven by evapotranspiration and recharge from the Zambezi River.

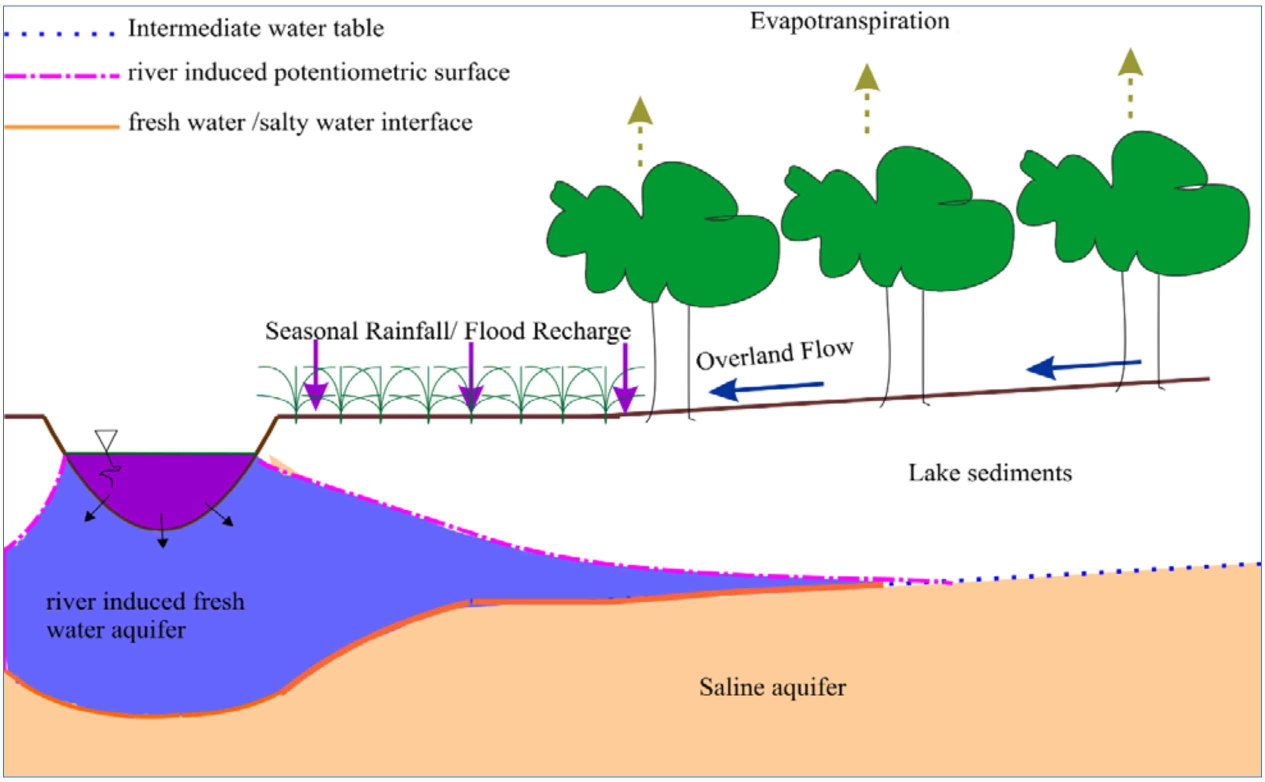

Figure 9: Conceptual model of surface water/ groundwater interaction in the Simalaha flood plain. The major drivers are conceptualised as seasonally varying water table in the Zambezi River, localised seasonal rainfall and flooding, overland flow and evapotranspiration.

In addition, the separation of the chargeability section (Figure 7b) mid-way into a well layered part (0-3,300 m) and a chequered part (3,300.6,600 m) appears to correlate well with the extents of the plain and forest areas. The layered chargeability section is in the plain whereas the chequered chargeability section is in the forest. The reason for the high chargeability values and their distribution is unknown.

3.5 Regional scale perspectives

The landscape of the Machile-Zambezi Basin comprises a southern central low lying area (elevation between 900 – 950 m amsl) surrounded by moderate relief hilly areas from southeast to southwest in a clockwise direction. The drainage network is such that all streams flow from the hilly areas into the low lying area and either terminate into alluvial fans or eventually end up into the Zambezi River. It is therefore likely that the groundwater regime in the upper reaches of the stream network is dominated by local flow systems with influent streams (Sophocleous, 2002). From the transition between the hilly areas and the low lying area up to the Zambezi River the topography exhibits very low gradient. Consequently the groundwater flow is probably dominated by intermediate and regional flow systems. These interact with a seasonal flood cycle whereby the river system is influent during flooding and effluent during the dry season (Main et al., 2008; Sophocleous, 2002). Thus surface water / groundwater interaction in the Machile-Zambezi Basin can be said to be driven by recharge in the high elevation areas and a mix of seasonally alternating exfiltration and infiltration in the moderate to low relief areas.

An evaluation of a satellite image encompassing the lower reaches of the Loanja River and the Kasaya area (Figure 10 a) shows the main channel of the Loanja River emerging from the high relief belt and broadening into an alluvial fan in the low relief region. Overlying the satellite image with a mean horizontal electrical resistivity map for depth interval 0-20 m from the airborne TEM (Figure 10 b.) shows that the alluvial fan is coincident with the higher electrical resistivity values. A similar observation can also be made about the Simalaha Floodplain (Chongo et al., 2015). The lack of borehole records along the Kasaya Transect makes it extremely difficult to constrain the geophysical result to geomorphological and hydro-chemical features. However Chongo et al. (2015) do give an interpretation of the regional electrical resistivity distribution based on textural and pore fluid considerations that in general associate high electrical resistivity values with coarser sediments and low groundwater salinity; and low electrical resistivity values with intercalations of finer and coarser sediments and high groundwater salinity as illustrated in Table 1 below.

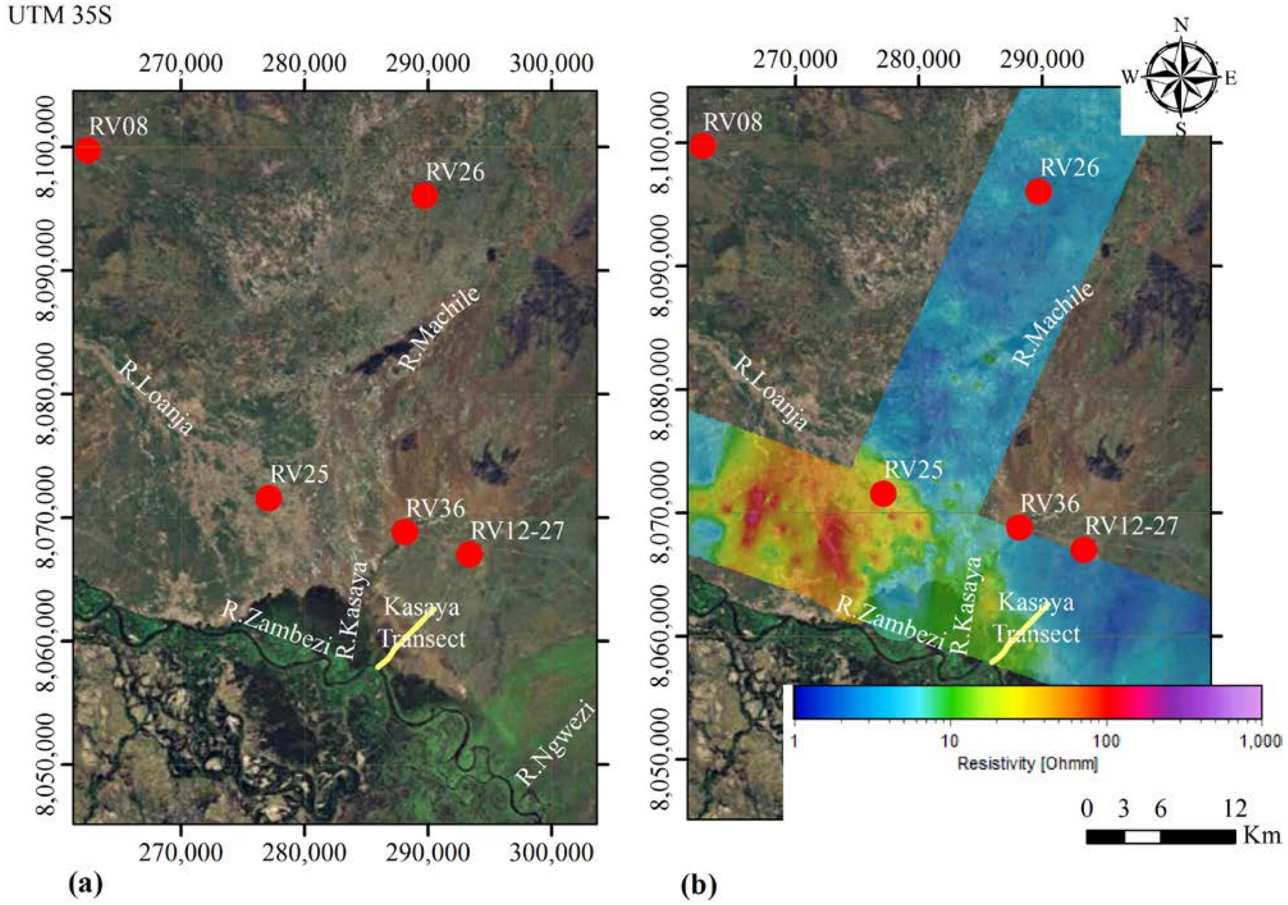

Figure 10: (a) Satellite imagery (ESRI worldly 2D) showing termination of Loanja River into an alluvial fan in the Sesheke area, south-western Zambia. (b) Superimposition of horizontal mean resistivity map for depth interval 0-20 m onto an ESRI worldly 2D Imagery.

Table 1: Correlation of formation electrical resistivity, pore water conductivity and lithology for available complete borehole records in the Machile-Zambezi Basin (Chongo et al., 2015).

Borehole	Location [UTM 35S]		Pore Water Conductivity [µS/cm]	Formation Resistivity[Ωm]	Lithology	Category
	Northing [m]	Easting [m]				
RV_31	8098183.40	237931.96	372.24	179.48	Sand	Freshwater
RV_08	8099759.76	262479.77	577.80	99.31	Clayey Sand and sandstone	Freshwater
RV_29	8076339.01	211449.36	459.53	32.75	Sandstone/ Basalt	Freshwater
RV_12_02	8137425.81	299048.19	466.58	32.52	Sand/ Sandstone	Freshwater
RV_36	8068825.60	288165.00	636.02	24.19	Sand/ Sandstone	Feshwater
RV_01	8070051.34	231262.64	2220.91	8.74	Sandy Clay	Salty water
RV_26	8096066.40	289747.90	4659.35	5.66	Clayey sand	Salty water

4 Conclusion

A combination of TEM and DCIP measurements processed under joint inversion provided insight into the nature of surface water / groundwater interaction on the northern bank of the Zambezi River at Kasaya in southern Zambia. To our knowledge, this is the first time that joint inversion of TEM and DCIP data has been conducted. The joint inversion showed a fresh water lens about 6.6 km in length from the edge of the Zambezi River. This was found to be about 60 m thick at the interface with the river and slowly thinned out further away from the river until it reached a thickness of about 22 m at the end of the transect line. The fresh water lens is postulated to have had been produced by a combination of river interaction with the aquifer and influenced by evapotranspiration. On a sub-regional scale, the hilly and higher elevation areas of the Machile Zambezi Basin act as recharge areas with influent streams, whereas the low lying areas interact with a seasonal flood cycle whereby the river system is influent during flooding and effluent during the dry season.

Finally, the combination of DCIP and TEM data in a joint inversion produced better inverse models with well resolved model parameters based on DOI considerations. The TEM method was better at resolving electrical resistivities and thicknesses for the deeper layers whereas the DC LCI produced inverse models with well resolved electrical resistivities and layer thicknesses in the shallow sub surface but could not resolve these parameters at well enough at depth. However the DC method provided more data density. Joint inversion of DCIP and TEM data thus produced a result with the benefits of both high spatial density and good determination of electrical resistivities and layer thicknesses both in the shallow subsurface and the deeper subsurface. Including IP data in the inversion had the added value of indicating the stratification and zones where fresh surface water has probably infiltrated into the sub surface and replaced salty groundwater.

Acknowledgements

We are grateful to the Governments of the Republic of Zambia and the Kingdom of Denmark for sponsoring this research under the capacity building initiative for the Zambian water sector though the University of Zambia. Special thanks also go to Dr. Chisengu Mdala, Lecturer in Geophysics at the University of Zambia and proprietor of Azurite Water Resources (Ltd) for allowing his field technician James Zulu to accompany us if the field to collect the CVES and TEM data and to Ingrid Mugamya at the UNZA IWRM Centre for logistical support. Furthermore we are grateful to Erik Lange from DTU for facilitating the meeting with Kurt Sørensen of SkyTEM that enabled us to borrow their WalkTEM instrument for our fieldwork. We would also like to thank Kebby Kapika (District Water Officer –Sesheke, Western Province, Zambia), Mweemba Sinkombo (District Water Officer -Nalolo, Western Province, Zambia) and the community at Kasaya for moral and physical support during the field measurements. Finally we would like to thank the Hydro-geophysics group at Aarhus University for assistance during processing and inversion of the TEM and CVES datasets.

References

ABEM(a), 2012. Terrameter LS User's Guide. ABEM Geophysics, Stockholm, p. 42.

ABEM(b), 2014. WalkTEM User's Guide. ABEM Geophysics, Stockholm, p. 42.

Aizebeokhai, A.P., 2010. 2D and 3D geoelectrical resistivity imaging: Theory and field design. SCIENTIFIC RESEARCH AND ESSAYS 5, 3592-3605.

Albouy, Y., Andrieux, P., Rakotondrasoa, G., Ritz, M., Descloitres, M., Join, J.L., Rasolomanana, E., 2001. Mapping coastal aquifers by joint inversion of DC and TEM soundings - Three case histories. Ground Water 39, 87-97.

Aristodemou, E., Thomas-Betts, A., 2000. DC resistivity and induced polarisation investigations at a waste disposal site and its environments. J. Appl. Geophys. 44, 275-302.

Auken, E., Christiansen, A.V., Jacobsen, B.H., Foged, N., Sorensen, K.I., 2005. Piecewise 1D laterally constrained inversion of resistivity data. Geophysical Prospecting 53, 497-506.

Auken, E., Christiansen, A.V., Kirkegaard, C., Fiandaca, G., Schamper, C., Behroozmand, A.A., Binley, A., Nielsen, E., Efferso, F., Christensen, N.B.i., Sorensen, K., Foged, N., Vignoli, G., 2014. An overview of a highly versatile forward and stable inverse algorithm for airborne, ground-based and borehole electromagnetic and electric data. Exploration Geophysics.

Banda, K.E., Jakobsen, R., Gottwein, P.B.-., Nyambe, I., Laier, T., Larsen, F., 2015. Identification and evaluation of hydro-geochemical processes in the groundwater environment of Machile Basin, western Zambia Unpublished results. Technical University of Denmark, 2500kgs-Lynby, Denmark, Lynby, Denmark, p. 50.

Banda, K.E., Jakobsenc, R., Gottwein, P.B.-., Murrayd, A.S., Nyambe, I., Larsen, F., 2014. The Lake Palaeo-Makgadikgadi in western Zambia: its formation and role in producing recent saline groundwater, Unpublished results. Geological Survey of Denmark and Greenland, p. 47.

Bauer, P., Supper, R., Zimmermann, S., Kinzelbach, W., 2006. Geoelectrical Imaging of Groundwater Salinisation in the Okavango Delta, Botswana. J. Appl. Geophys. 60, 126-141.

Behroozmand, A.A., Auken, E., Fiandaca, G., Christiansen, A.V., 2012. Improvement in MRS parameter estimation by joint and laterally constrained inversion of MRS and TEM data. Geophysics 77.

Bertin, J., Loeb, J., 1969. Transients and field behaviour in induced polarization. Geophysical Prospecting 17, 488-510.

Binley, A., Kemna, A., 2006. DC Resistivity and Induced Polarization Methods, in: Rubin, Y., Hubbard, S.S. (Eds.), Hydrogeophysics. Springer.

Brodie, R., Sundaram, B., Tottenham, R., Hostetler, S., Ransley, T., 2007. An Overview of Tools for Assessing Groundwater-Surface Water Connectivity, in: Forestry, D.o.A.i.a. (Ed.). Bureau of Rural Sciences, Canberra. .

Chongo, M., Christiansen, A.V., Tembo, A., Banda, K.E., Nyambe, I.A., Larsen, F., Bauer-Gottwein, P., 2015. Airborne and Ground based Transient Electromagnetic Mapping of Groundwater Salinity in the Machile-Zambezi Basin, South-western Zambia. . Near Surface Geophysics 13, 383 - 395.

Christiansen, A.V., Auken, E., 2012. A global measure for depth of investigation. Geophysics 77.

Christiansen, A.V., Auken, E., Foged, N., Sorensen, K.I., 2007. Mutually and laterally constrained inversion of CVES and TEM data: a case study. Near Surface Geophysics 5, 115-123.

Christiansen, A.V., Esben, A., Sørensen, K., 2006. The Transient Electromagnetic Method, in: Kirsch, R. (Ed.), Groundwater Geophysics, A Tool for Hydrogeology. Springer, Flintbek, Germany.

Dahlin, T., 2001. The development of DC resistivity imaging techniques. Computers and Geosciences 27, 1019-1029.

Dahlin, T., Leroux, V., Nissen, J., 2002. Measuring techniques in induced polarisation imaging. J. Appl. Geophys. 50, 279-298.

Dahlin, T., Zhou, B., 2006. Multiple-gradient array measurements for multichannel 2D resistivity imaging. Near Surface Geophysics 4, 113-123.

Danielsen, J.E., Auken, E., Jørgensen, F., Søndergaard, V., Sørensen, K.I., 2003. The application of the transient electromagnetic method in hydrogeophysical surveys. J. Appl. Geophys. 53, 181-198.

Danielsen, J.E., Dahlin, T., Owen, R., Mangeya, P., Auken, E., 2007. Geophysical and Hydrogeologic Investigation of Groundwater in the Karoo Stratigraphic Sequence at Sawmills in Nothern Matebeleland, Zimbabwe: A Case History. Hydrogeology Journal 15, 945-960.

ESRI, 2014. World Imagery.

Ezersky, M., Legchenko, A., Al-Zoubi, A., Levi, E., Akkawi, E., Chalikakis, K., 2011. TEM study of the geoelectrical structure and groundwater salinity of the Nahal Hever sinkhole site, Dead Sea shore, Israel. J. Appl. Geophys. 75, 99-112.

Fiandaca, G., Auken, E., Christiansen, A.V., Gazoty, A., 2012. Time-domain-induced polarization: Full-decay forward modeling and 1D laterally constrained inversion of Cole-Cole parameters. Geophysics 77, E213-E225.

Fiandaca, G., Ramm, J., Binley, A., Gazoty, A., Christiansen, A.V., Auken, E., 2013. Resolving spectral information from time domain induced polarization data through 2-D inversion. GEOPHYSICAL JOURNAL INTERNATIONAL 192, 631-646.

Gazoty, A., Fiandaca, G., Pedersen, J., Auken, E., Christiansen, A.V., 2012a. Mapping of landfills using time-domain spectral induced polarization data: the Eskelund case study. Near Surface Geophysics 10, 575-586.

Gazoty, A., Fiandaca, G., Pedersen, J., Auken, E., Christiansen, A.V., 2013. Data repeatability and acquisition techniques for time-domain spectral induced polarization. Near Surface Geophysics 11, 391-406.

Gazoty, A., Fiandaca, G., Pedersen, J., Auken, E., Christiansen, A.V., Pedersen, J.K., 2012b. Application of time domain induced polarization to the mapping of lithotypes in a landfill site. Hydrology and Earth System Sciences 16, 1793-1804.

Geonics, 2006. PROTEM 47D Operating Manual for 20/30 Gate Model. Geonics Limited, Ontario, Canada.

GEOTECH, 2011. Survey and logistcs report on a helicopter borne versatile time domain electromagnetic survey on the Zambezi River Basin Kazungula Zambia for Ministry of Energy and Water Development (Republic of Zambia). GEOTECH AIRBORNE LIMITED, West Indies, p. 20.

Guerin, R., Descloitres, M., Coudrain, A., Talbi, A., Gallaire, R., 2001. Geophysical surveys for identifying saline groundwater in the semi-arid region of the central Altiplano, Bolivia. Hydrol. Process. 15, 3287-3301.

Harthill, N., 1976. Time-Domain Electromagnetic Sounding. IEEE Transactions on Geoscience Electronics 14, 256-260.

Johnson, I.M., 1984. Spectral induced polarization parameters as determined through time-domain measurements. Geophysics 49.

Kameyama, N., 2003. Completion Report: JICA borehole drilling project-Sesheke. Ministry of Energy and Water Development, Lusaka.

Kirsch, R., 2009. Groundwater geophysics : a tool for hydrogeology.

Loke, M.H., 1999. Electrical Imaging Surveys for Environmental and Engineering Studies, A Practical Guide to 2-D and 3-D Surveys, Malaysia.

Loke, M.H., Chambers, J.E., Rucker, D.F., Kuras, O., Wilkinson, P.B., 2013. Recent developments in the direct-current geoelectrical imaging method. J. Appl. Geophys. 95, 135-156.

Main, M.P.L., Moore, A.E., Williams, H.B., Cotterill, F.P.D., 2008. The Zambezi River. Large Rivers: Geomorphology and Management, 311-332.

Marescot, L., Monnet, R., Chapellier, D., 2008. Resistivity and induced polarization surveys for slope instability studies in the Swiss Alps. ENGINEERING GEOLOGY 98, 18-28.

Milosevic, N., Thomsen, N.I., Juhler, R.K., Albrechtsen, H.J., Bjerg, P.L., 2012. Identification of discharge zones and quantification of contaminant mass discharges into a local stream from a landfill in a heterogeneous geologic setting. Journal of Hydrology 446, 13-23.

Mualem, Y., Friedman, S.P., 1991. THEORETICAL PREDICTION OF ELECTRICAL-CONDUCTIVITY IN SATURATED AND UNSATURATED SOIL. Water Resources Research 27, 2771-2777.

Nabighian, M.N., 1991. Electromagnetic Methods in Applied Geophysics Vol. 2, Electromagnetic Methods in Applied Geophysics Vol. 2.

Nassir, S.S.A., Loke, M.H., Lee, C.Y., Nawawi, M.N.M., 2000. Salt-water intrusion mapping by geoelectrical imaging surveys. Geophysical Prospecting 48, 647-661.

Oldenburg, D.W., Li, Y.G., 1999. Estimating depth of investigation in dc resistivity and IP surveys. Geophysics 64, 403-416.

Pelton, W.H., Ward, S.H., Hallof, P.G., Sill, W.R., Nelson, P.H., 1978. Mineral discrimination and removal of inductive coupling with multifrequency IP. Geophysics 43, 588-609.

Rhoades, J.D., Kandiah, A., Mashali, A.M., 1992. The use of saline waters for crop production - FAO irrigation and drainage paper 48. FOOD AND AGRICULTURE ORGANIZATION OF THE UNITED NATIONS, Rome.

Rhoades, J.D., Manteghi, N.A., Shouse, P.J., Alves, W.J., 1989. SOIL ELECTRICAL-CONDUCTIVITY AND SOIL-SALINITY - NEW FORMULATIONS AND CALIBRATIONS. SOIL SCIENCE SOCIETY OF AMERICA JOURNAL 53, 433-439.

Roy, A., Apparao, A., 1971. DEPTH OF INVESTIGATION IN DIRECT CURRENT METHODS. Geophysics 36, 943-959.

Rubin, Y., Hubbard, S.S., 2006. Hydrogeophysics. Springer.

Shalem, Y., Weinstein, Y., Levi, E., Herut, B., Goldman, M., Yechieli, Y., 2014. The extent of aquifer salinization next to an estuarine river, an example from the eastern mediterranean. Hydrogeology Journal.

Shanafield, M., Cook, P.G., 2014. Transmission losses, infiltration and groundwater recharge through ephemeral and intermittent streambeds: A review of applied methods. Journal of Hydrology 511, 518-529.

Slater, L.D., Lesmes, D., 2002. IP interpretation in environmental investigations. Geophysics 67, 77-88.

Sonkamble, S., Kumar, V.S., Amarender, B., Dhunde, P.M., Sethurama, S., Kumar, K.R., 2014. Delineation of fresh aquifers in tannery belt for sustainable development - A case study from southern India. J. Geol. Soc. India 83, 279-289.

Sophocleous, M., 2002. Interactions between groundwater and surface water: the state of the science. Hydrogeology Journal 10, 52-67.

Spies, B.R., 1989. Depth of investigation in electromagnetic sounding methods. Geophysics 54, 872-888.

Titov, K., Komarov, V., Tarasov, V., Levitski, A., 2002. Theoretical and experimental study of time domain-induced polarization in water-saturated sands. J. Appl. Geophys. 50, 417-433.

Vaudelet, P., Schmutz, M., Pessel, M., Franceschi, M., Guerin, R., Atteia, O., Blondel, A., Ngomseu, C., Galaup, S., Rejiba, F., Begassat, P., 2011. Mapping of contaminant plumes with geoelectrical methods. A case study in urban context. J. Appl. Geophys. 75, 738-751.

Vilhelmsen, T.N., Behroozmand, A.A., Christensen, S., Nielsen, T.H., 2014. Joint inversion of aquifer test, MRS, and TEM data. Water Resources Research 50, 3956-3975.

Weller, A., Slater, L., Nordsiek, S., 2013. On the relationship between induced polarization and surface conductivity: Implications for petrophysical interpretation of electrical measurements. Geophysics 78, D315-D325.

Westbrook, S.J., Rayner, J.L., Davis, G.B., Clement, T.P., Bjerg, P.L., Fisher, S.T., 2005. Interaction between shallow groundwater, saline surface water and contaminant discharge at a seasonally and tidally forced estuarine boundary. Journal of Hydrology 302, 255-269.

Winter, T.C., 1999. Relation of streams, lakes, and wetlands to groundwater flow systems. Hydrogeology Journal 7, 28-45.

Xue, G.-q., Bai, C.-y., Yan, S., Greenhalgh, S., Li, M.-f., Zhou, N.-n., 2012. Deep sounding TEM investigation method based on a modified fixed central-loop system. J. Appl. Geophys. 76, 23-32.

Zarroca, M., Bach, J., Linares, R., Pellicer, X.M., 2011. Electrical methods (VES and ERT) for identifying, mapping and monitoring different saline domains in a coastal plain region (Alt Emporda, Northern Spain). Journal of Hydrology 409, 407-422.

Zarroca, M., Linares, R., Rodellas, V., Garcia-Orellana, J., Roqué, C., Bach, J., Masqué, P., 2014. Delineating coastal groundwater discharge processes in a wetland area by means of electrical resistivity imaging, 224Ra and 222Rn. Hydrol. Process. 28, 2382-2395.

Zarroca, M., Linares, R., Velásquez-López, P.C., Roqué, C., Rodríguez, R., 2015. Application of electrical resistivity imaging (ERI) to a tailings dam project for artisanal and small-scale gold mining in Zaruma-Portovelo, Ecuador. J. Appl. Geophys. 113, 103-113.

Zhou, S., Yuan, X., Peng, S., Yue, J., Wang, X., Liu, H., Williams, D.D., 2014. Groundwater-surface water interactions in the hyporheic zone under climate change scenarios. Environmental Science and Pollution Research.